J|A|C|S
ARTICLES
Published on Web 11/22/2006

Hydrogen-Bonded Porous Coordination Polymers: Structural Transformation, Sorption Properties, and Particle Size from Kinetic Studies

Kazuhiro Uemura,*,† Kazuya Saito,‡ Susumu Kitagawa,§ and Hidetoshi Kita†

Contribution from the Environmental Science and Engineering, Graduate School of Science and Engineering, Yamaguchi University, Tokiwadai 2-16-1, Ube-shi, Yamaguchi 755-8611, Japan, Department of Chemistry, Graduate School of Pure and Applied Sciences, University of Tsukuba, Tsukuba, Ibaraki 305-8571, Japan, and Department of Synthetic Chemistry and Biological Chemistry, Graduate School of Engineering, Kyoto University, Katsura, Nishigyo-ku, Kyoto 615-8510, Japan

Received June 13, 2006; E-mail: kazu-u@yamaguchi-u.ac.jp

Abstract: Three new coordination polymers, $[CoCl_2(4\text{-pmna})_2]_n$ (**1**), $\{[Co(NCS)_2(4\text{-pmna})_2]\cdot 2Me_2CO\}_n$ (**2** ⊃ **2Me$_2$CO**), and $\{[Co(4\text{-pmna})_2(H_2O)_2](NO_3)_2\cdot 2CH_3OH\}_n$ (**3** ⊃ **2H$_2$O·2MeOH**) (4-pmna = *N*-(pyridin-4-ylmethyl)nicotinamide), have been synthesized and characterized using single-crystal X-ray diffraction. The cobalt(II) atoms are bridged by 4-pmna ligands in all three compounds to form double-stranded one-dimensional "repeated rhomboid-type" chains with rectangular-shaped cavities. In **1**, each chain slips and obstructs the neighboring cavities so that there are no guest-incorporated pores. Both **2** ⊃ **2Me$_2$CO** and **3** ⊃ **2H$_2$O·2MeOH** do not have such a staggered arrangement and have pores that can be filled with a guest molecule. Compound **3** ⊃ **2H$_2$O·2MeOH** traps guest molecules with multiple hydrogen bonds and shows a reversible structural rearrangement during adsorption and desorption. The new crystalline compound, **3**, is stabilized by forming hydrogen bonds with the amide moieties of the 4-pmna ligands and was characterized using infrared spectroscopy. The clathration enthalpy of the reaction **3** + $2H_2O$(l) + 2MeOH(l) ⇄ **3** ⊃ **2H$_2$O·2MeOH** (≈35 kJ/mol) was estimated from differential scanning calorimetry data by considering the vaporization enthalpies of H_2O and MeOH. The desorption process of **3** ⊃ **2H$_2$O·2MeOH** → **3** follows a single zero-order reaction mechanism under isothermal conditions. The activation energy of ca. 100 kJ/mol was obtained by plotting the logarithm of the reaction time for the same reacted fraction versus the reciprocal of the temperature. Moreover, the distribution of the one-dimensional channels in **3** ⊃ **2H$_2$O·2MeOH** was estimated using the observation that the reaction rate is directly proportional to the total sectional area.

Introduction

Soft porous materials, whose pore sizes and shapes are deformed with guest molecule adsorption and desorption, are now recognized as a new class of functional materials. These materials have already been studied as organic zeolites[1] and mononuclear complexes,[2] as well as coordination polymers.[3−5] During the last few decades, a large number of coordination polymers have been designed and synthesized successfully through the combination of organic ligands (spacers) and metal ions (nodes).[6] Since one of the main functional goals of coordination polymer research has been to obtain a stable porous framework, rigid three-dimensional coordination polymers have resulted from the formation of stiff bridging ligands.[7] However,

* To whom correspondence should be addressed. Tel: 81-836-85-9663. Fax: 81-836-85-9601.
† Yamaguchi University.
‡ University of Tsukuba.
§ Kyoto University.

(1) For example of flexible organic zeolites; (a) Miyata, M.; Shibakami, M.; Chirachanchai, S.; Takemoto, K.; Kasai, N.; Miki, K. *Nature* **1990**, *343*, 446−447. (b) Bourne, S. A.; Nassimbeni, L. R.; Toda, F. *J. Chem. Soc., Perkin Trans. 2* **1991**, *1335*−1341. (c) Barbour, L. J.; Caira, M. R.; Coetzee, A.; Nassimbeni, L. R. *J. Chem. Soc,. Perkin Trans. 2* **1995**, 1345−1349. (d) Ung, A. T.; Gizachew, D.; Bishop, R.; Scudder, M. L.; Dance, I. G.; Craig, D. C. *J. Am. Chem. Soc.* **1995**, *117*, 8745−8756. (e) Endo, K.; Sawaki, T.; Koyanagi, M.; Kobayashi, K.; Masuda, H.; Aoyama, Y. *J. Am. Chem. Soc.* **1995**, *117*, 8341−8352. (f) Endo, K.; Koike, T.; Sawaki, T.; Hayashida, O.; Masuda, H.; Aoyama, Y. *J. Am. Chem. Soc.* **1997**, *119*, 4117−4122. (g) Thaimattam, R.; Xue, F.; Sarma, J. A. R. P.; Mak, T. C. W.; Desiraju, G. R. *J. Am. Chem. Soc.* **2001**, *123*, 4432−4445. (h) Atwood, J. L.; Barbour, L. J.; Jerga, A.; Schottel, B. L. *Science* **2002**, *298*, 1000−1002.

(2) Recent flexible porous complexes: (a) Atwood, J. L.; Davies, J. E. D.; MacNicol, D. D. *Inclusion Compounds*; Academic Press: London, 1984; Vol. 1. (b) Manakov, A. Y.; Soldatov, D. V.; Ripmeester, J. A.; Lipkowski, J. *J. Phys. Chem. B* **2000**, *104*, 12111−12118. (c) Soldatov, D. V.; Moudrakovski, I. L.; Ratcliffe, C. I.; Dutrisac, R.; Ripmeester, J. A. *Chem. Mater.* **2003**, *15*, 4810−4818. (d) Soldatov, D. V.; Enright, G. D.; Ripmeester, J. A. *Cryst. Growth Des.* **2004**, *4*, 1185−1194. (e) Kawamoto, R.; Uchida, S.; Mizuno, N. *J. Am. Chem. Soc.* **2005**, *127*, 10560−10567.

(3) Reviews for flexible porous coordination polymers: (a) Bradshaw, D.; Claridge, J. B.; Cussen, E. J.; Prior, T. J.; Rosseinsky, M. J. *Acc. Chem. Res.* **2005**, *38*, 273−282. (b) Kitagawa, S.; Uemura, K. *Chem. Soc. Rev.* **2005**, *34*, 109−119. (c) Navarro, J. A. R.; Barea, E.; Galindo, M. A.; Salas, J. M.; Romero, M. A.; Quiros, M.; Masciocchi, N.; Galli, S.; Sironi, A.; Lippert, B. *J. Solid State Chem.* **2005**, *178*, 2436−2451. (d) Fletcher, A. J.; Thomas, K. M.; Rosseinsky, M. J. *J. Solid State Chem.* **2005**, *178*, 2491−2510. (e) Shimizu, G. K. H. *J. Solid State Chem.* **2005**, *178*, 2519−2526. (f) Uemura, K.; Matsuda, R.; Kitagawa, S. *J. Solid State Chem.* **2005**, *178*, 2420−2429.

10.1021/ja064152r CCC: $33.50

recently, several soft porous coordination polymers have been found that exhibit framework transformation on the adsorption or desorption of guest molecules,[2−5] which have been recognized as being "flexible porous coordination polymers."

These flexible porous coordination polymers are regarded as being bistable frameworks whose state oscillates between two counterparts, as shown in eq 1,

$$\mathrm{H} + n\mathrm{G} \rightleftarrows \mathrm{H} \supset n\mathrm{G},\ \Delta H_{\mathrm{clath}} \qquad (1)$$

where H is the apohost, G is a guest molecule, n is the stoichiometry of the accommodated guest molecule versus that of the apohost, and $\Delta H_{\mathrm{clath}}$ is the enthalpy of clathration. In other words, flexible porous coordination polymers have different frameworks: the "H" (apohost) and the "H ⊃ nG" (host with guest) framework. Although flexible porous coordination polymers can provide new classes of functional materials, such as those with highly selective guest accommodation[4a,5a] and those with magnetic modulation,[8] a deeper understanding of these materials is required. In particular, the guest adsorption and desorption mechanism is much more complicated than that observed in conventional rigid porous materials.

The analysis of the adsorption and desorption of rigid porous coordination polymers is similar to that used for zeolites. However, flexible porous coordination polymers offer unique observational data, such as their gate-pressure and a large hysteresis loop.[5,9] The kinetic and thermodynamic approaches to flexible porous coordination polymers make analysis of these mechanisms clearer and provide detailed information. Nevertheless, most published studies have focused on architectural design and the construction of flexible porous coordination polymers, while analysis of the mechanism of guest adsorption and desorption has been largely overlooked.

For such a systematic study, we have previously proposed contrivances for flexible frameworks[3b] by introducing hydrogen bonds that have flexible lengths and angles[6a,10] compared to covalent and coordination bonds. The py-CONH-X-py ligands (where CONH = amide group and X = spacer) are suitable for the rational introduction of hydrogen bonds, e.g., in $\{[Co(NCS)_2(3\text{-pia})_2]\cdot 4Me_2CO\}_n$[5a,c] and $\{[Co(NCS)_2(4\text{-peia})_2]\cdot 4Me_2CO\}_n$[5b] (where 3-pia = *N*-3-pyridylisonicotinamide and 4-peia = *N*-(2-pyridin-4-yl-ethyl)-isonicotinamide), which show a reversible adsorption and desorption of Me_2CO molecules along with a framework transformation, in which the amide moiety forms in different types of hydrogen bonds.

Based on this background, we show the synthesis and structures of novel repeated rhomboid-type coordination polymers, $[CoCl_2(4\text{-pmna})_2]_n$ (**1**), $\{[Co(NCS)_2(4\text{-pmna})_2]\cdot 2Me_2CO\}_n$ (**2 ⊃ 2Me$_2$CO**), and $\{[Co(4\text{-pmna})_2(H_2O)_2](NO_3)_2\cdot 2CH_3OH\}_n$ (**3 ⊃ 2H$_2$O·2MeOH**), by selecting the py-CONH-X-py ligand to be 4-pmna (*N*-(pyridin-4-ylmethyl)nicotinamide) and regulating each network motif with hydrogen bonds between the amide moieties and the anions. In particular, **3 ⊃ 2H$_2$O·2MeOH** shows a reversible structural rearrangement, which was investigated in detail using kinetic and thermodynamic analysis, shedding light on the relationship between the particle size and the desorption kinetics.

Experimental Section

Materials. For 4-pmna, nicotinic chloride hydrochloride and 4-pycolylamine were obtained from Tokyo Kasei Industrial Co. $CoCl_2\cdot 6H_2O$ and $Co(NO_3)_2\cdot 6H_2O$ were obtained from Wako Co. $Co(SCN)_2$ was obtained from Aldrich Chemical Co.

Synthesis of *N*-(Pyridin-4-ylmethyl)nicotinamide (4-pmna). This ligand was readily prepared by the reaction of nicotinic chloride hydrochloride (13 g, 73 mmol) with 4-pycolylamine (7.4 mL, 73 mmol) in dry tetrahydrofuran (250 mL) in the presence of triethylamine (21 mL, 150 mmol) under N_2. The product was recrystallized from acetone/hexane to give an 83% yield (8.3 g): ^{1}H NMR (DMSO) δ 4.51 (d, J = 6.0 Hz, 2H), δ 7.32 (d, J = 5.5 Hz, 2H), δ 7.52 (dd, J = 8.0 Hz; 5.0 Hz, 1H), δ 8.23 (d, J = 8.0 Hz, 1H), δ 8.51 (d, J = 5.5 Hz, 2H), δ 8.72 (d, J = 5.0 Hz, 1H), δ 9.06 (s, 1H), δ 9.31 (t, J = 6.0 Hz, 1H). Anal. Calcd for $C_{12}H_{11}N_3O$: C, 67.59; H, 5.20; N, 19.71. Found: C, 67.33; H, 5.44; N, 19.53.

$[CoCl_2(4\text{-pmna})_2]_n$ (1). In order to obtain the single crystals, in a glass tube (5 mL, 10 mm i.d.) a solvent of ethanol/chloroform (v/v 19:1) was carefully layered onto a methanol/chloroform mixed (v/v 9:1) solution (1.5 mL) of $CoCl_2\cdot 6H_2O$ (17.8 mg, 0.075 mmol), and then an ethanol solution (1.5 mL) of 4-pmna (32 mg, 0.15 mmol) was carefully layered onto a ethanol/chloroform (v/v 19:1) layer. Violet crystals of **1** suitable for X-ray diffraction (XRD) were obtained (yield: 86%). Anal. Calcd for for $C_{24}H_{22}Cl_2CoN_6O_2$: C, 51.82; H, 3.99; N, 15.11. Found: C, 51.63; H, 4.00; N, 15.20.

$\{[Co(NCS)_2(4\text{-pmna})_2]\cdot 2Me_2CO\}_n$ (2 ⊃ 2Me$_2$CO). In order to obtain the single crystals, in glass tube (5 mL, 10 mm i.d.) a solvent of

(4) Recent flexible porous coordination polymers: (a) Makinen, S. K.; Melcer, N. J.; Parvez, M.; Shimizu, G. K. H. *Chem. Eur. J.* **2001**, *7*, 5176−5182. (b) Soldatov, D. V.; Ripmeester, J. A. *Chem. Eur. J.* **2001**, *7*, 2979−2994. (c) Soldatov, D. V.; Enright, G. D.; Ripmeester, J. A. *Chem. Mater.* **2002**, *14*, 348−356. (d) Cussen, E. J.; Claridge, J. B.; Rosseinsky, M. J.; Kepert, C. J. *J. Am. Chem. Soc.* **2002**, *124*, 9574−9581. (e) Takamizawa, S.; Nakata, E.-i.; Yokoyama, H.; Mochizuki, K.; Mori, W. *Angew. Chem., Int. Ed.* **2003**, *42*, 4331−4334. (f) Maji, T. K.; Uemura, K.; Chang, H. C.; Matsuda, R.; Kitagawa, S. *Angew. Chem., Int. Ed.* **2004**, *43*, 3269−3272. (g) Lee, E. Y.; Suh, M. P. *Angew. Chem., Int. Ed.* **2004**, *43*, 2798−2801. (h) Choi, H. J.; Suh, M. P. *J. Am. Chem. Soc.* **2004**, *126*, 15844−15851. (i) Zeng, M. H.; Feng, X. L.; Chen, X. M. *Dalton Trans.* **2004**, 2217−2223. (j) Kondo, M.; Irie, Y.; Shimizu, Y.; Miyazawa, M.; Kawaguchi, H.; Nakamura, A.; Naito, T.; Maeda, K.; Uchida, F. *Inorg. Chem.* **2004**, *43*, 6139−6141. (k) Wu, C. D.; Lin, W. *Angew. Chem., Int. Ed.* **2005**, *44*, 1958−1961. (l) Takaoka, K.; Kawano, M.; Tominaga, M.; Fujita, M. *Angew. Chem., Int. Ed.* **2005**, *44*, 2151−2154. (m) Halder, G. J.; Kepert, C. J. *J. Am. Chem. Soc.* **2005**, *127*, 7891−7900.

(5) (a) Uemura, K.; Kitagawa, S.; Kondo, M.; Fukui, K.; Kitaura, R.; Chang, H. C.; Mizutani, T. *Chem. Eur. J.* **2002**, *8*, 3586−3600. (b) Uemura, K.; Kitagawa, S.; Fukui, K.; Saito, K. *J. Am. Chem. Soc.* **2004**, *126*, 3817−3828 and references therein. (c) Uemura, K.; Kitagawa, S.; Saito, K.; Fukui, K.; Matsumoto, K. *J. Therm. Anal. Calorim.* **2005**, *81*, 529−532.

(6) (a) Desiraju, G. R. *Angew. Chem., Int. Ed.* **1995**, *34*, 2311−2327. (b) Batten, S. R.; Robson, R. *Angew. Chem., Int. Ed.* **1998**, *37*, 1460−1494. (c) Hagrman, P. J.; Hagrman, D.; Zubieta, J. *Angew. Chem., Int. Ed.* **1999**, *38*, 2638−2684. (d) Aakeroy, C. B.; Beatty, A. M. *Aust. J. Chem.* **2001**, *54*, 409−421. (e) Khlobystov, A. N.; Blake, A. J.; Champness, N. R.; Lemenovskii, D. A.; Majouga, A. G.; Zyk, N. V.; Schroder, M. *Coord. Chem. Rev.* **2001**, *222*, 155−192. (f) Zaworotko, M. J. *Chem. Commun.* **2001**, 1−9. (g) Moulton, B.; Zaworotko, M. J. *Chem. Rev.* **2001**, *101*, 1629−1658. (h) Kitaura, R.; Kitagawa, S.; Kubota, Y.; Kobayashi, T. C.; Kindo, K.; Mita, Y.; Matsuo, A.; Kobayashi, M.; Chang, H. C.; Ozawa, T. C.; Suzuki, M.; Sakata, M.; Takata, M. *Science* **2002**, *298*, 2358−2361. (i) Matsuda, R.; Kitaura, R.; Kitagawa, S.; Kubota, Y.; Belosludov, R. V.; Kobayashi, T. C.; Sakamoto, H.; Chiba, T.; Takata, M.; Kawazoe, Y.; Mita, Y. *Nature* **2005**, *436*, 238−241.

(7) (a) Yaghi, O. M.; O'Keeffe, M.; Ockwig, N. W.; Chae, H. K.; Eddaoudi, M.; Kim, J. *Nature* **2003**, *423*, 705−714. (b) Kitagawa, S.; Kitaura, R.; Noro, S.-i. *Angew. Chem., Int. Ed.* **2004**, *43*, 2334−2375. (c) Ferey, G.; Mellot-Dranznieks, C.; Serre, C.; Millange, F. *Acc. Chem. Res.* **2005**, *38*, 217−225.

(8) (a) Larionova, J.; Chavan, S. A.; Yakhmi, J. V.; Froystein, A. G.; Sletten, J.; Sourisseau, C.; Kahn, O. *Inorg. Chem.* **1997**, *36*, 6374−6381. (b) Usuki, N.; Ohba, M.; Okawa, H. *Bull. Chem. Soc. Jpn.* **2002**, *75*, 1693−1698. (c) Halder, G. J.; Kepert, C. J.; Moubaraki, B.; Murray, K. S.; Cashion, J. D. *Science* **2002**, *298*, 1762−1765. (d) Maspoch, D.; Ruiz-molina, D.; Wurst, K.; Domingo, N.; Cavallini, M.; Biscarini, F.; Tejada, J.; Rovira, C.; Veciana, A. J. *Nature Mater.* **2003**, *2*, 190−195.

(9) (a) Li, D.; Kaneko, K. *Chem. Phys. Lett.* **2001**, *335*, 50−56. (b) Kitaura, R.; Fujimoto, K.; Noro, S.-i.; Kondo, M.; Kitagawa, S. *Angew. Chem., Int. Ed.* **2002**, *41*, 133−135. (c) Seki, K. *Phys. Chem. Chem. Phys.* **2002**, *4*, 1968−1971.

(10) Steiner, T. *Angew. Chem., Int. Ed.* **2002**, *41*, 48−76.

Table 1. Crystal Data and Structure Refinement of $[CoCl_2(4\text{-pmna})_2]_n$ (**1**), $\{[Co(NCS)_2(4\text{-pmna})_2]\cdot 2Me_2CO\}_n$ (**2** ⊃ **2Me$_2$CO**), and $\{[Co(4\text{-pmna})_2(H_2O)_2](NO_3)_2\cdot 2CH_3OH\}_n$ (**3** ⊃ **2H$_2$O·2MeOH**)

compd	**1**	**2** ⊃ **2Me$_2$CO**	**3** ⊃ **2H$_2$O·2MeOH**
chemical formula	$C_{24}H_{22}Cl_2CoN_6O_2$	$C_{32}H_{22}CoN_8O_4S_2$	$C_{26}H_{28}CoN_8O_{12}$
formula weight	556.32	705.63	703.49
crystal system	triclinic	monoclinic	triclinic
space group	$P\bar{1}$	$P2_1/n$	$P\bar{1}$
T (K)	293	293	213
unit cell dims			
a (Å)	7.899(7)	11.371(2)	8.0720(7)
b (Å)	8.782(7)	10.063(1)	9.760(1)
c (Å)	8.980(8)	15.5356(4)	11.260(1)
α (deg)	84.70(2)	90	107.235(5)
β (deg)	81.32(2)	104.6391(7)	104.600(6)
γ (deg)	82.50(2)	90	101.293(3)
V (Å^3)	608.8(9)	1720.0(4)	784.0(1)
Z	1	2	1
D_c (g cm^{-1})	1.517	1.362	1.490
μ (Mo Kα) (mm^{-1})	0.959	0.668	0.622
F(000)	285	722	363
2θ range (deg)	5.5−55.0	5.5−55.0	5.5−53.4
GOF	1.691	1.998	1.901
R_1,[a] wR_2[b] [$I > 2\sigma(I)$]	0.041, 0.181	0.064, 0.208	0.050, 0.172
R_1,[a] wR_2[b] (all data)	0.041, 0.183	0.065, 0.225	0.051, 0.193

[a] $R = \Sigma||F_o| - |F_c||/\Sigma|F_o|$. [b] $R_w = \{\Sigma w[(F_o^2 - F_c^2)^2]/[(\Sigma wF_o^2)^2]\}^{1/2}$.

ethanol/chloroform (v/v 19:1) was carefully layered onto an acetone/chloroform mixed (v/v 9:1) solution (1.5 mL) of $Co(SCN)_2$ (6.6 mg, 0.038 mmol), and then an ethanol solution (1.5 mL) of 4-pmna (16 mg, 0.075 mmol) was carefully layered onto a ethanol/chloroform (v/v 19:1) layer. Red crystals of **2** ⊃ **2Me$_2$CO** suitable for XRD were obtained (yield: 88%). For elemental analysis these crystals were collected and dried in vacuo at 373 K for 20 h. Anal. Calcd for for $C_{26}H_{22}CoN_8O_2S_2$: C, 51.91; H, 3.69; N, 18.63. Found: C, 51.18; H, 3.58; N 18.17.

$\{[Co(4\text{-pmna})_2(H_2O)_2](NO_3)_2\cdot 2CH_3OH\}_n$ (3 ⊃ 2H$_2$O·2MeOH). In order to obtain the single crystals, in a glass tube (5 mL, 10 mm i.d.) a solvent of ethanol/chloroform (v/v 19:1) was carefully layered onto a methanol/chloroform mixed (v/v 9:1) solution (1.5 mL) of $Co(NO_3)_2\cdot 6H_2O$ (21.8 mg, 0.075 mmol), and then an ethanol solution (1.5 mL) of 4-pmna (32 mg, 0.15 mmol) was carefully layered onto a ethanol/chloroform (v/v 19:1) layer. Orange crystals of **3** ⊃ **2H$_2$O·2MeOH** suitable for XRD were obtained (yield: 21%). For elemental analysis these crystals were collected and dried in vacuo at 373 K for 20 h. Anal. Calcd for $C_{24}H_{22}CoN_8O_8$: C, 47.30; H, 3.64; N, 18.39. Found: C, 46.55; H, 4.02; N 18.25. The microcrystalline sample of **3** ⊃ **2H$_2$O·2MeOH** was prepared in the same solvent, and the crystallinity was checked by X-ray powder diffraction as shown in Figure S1 (Supporting Information).

Physical Measurements. Ultraviolet−visible reflection spectra were recorded on a Hitachi U-3500 spectrophotometer over the range 400−800 nm at room temperature. Infrared (IR) spectra were recorded on a Perkin-Elmer 2000 FT-IR spectrophotometer with samples prepared as a Nujol mull. Thermal gravimetry (TG) and differential thermal analysis were carried out with a Rigaku Instrument TG8120 in a nitrogen flow (50 mL/min). Differential scanning calorimetry (DSC) was carried out with a Rigaku Instrument TG8120 in a nitrogen flow (50 mL/min), and the heats of desorption were calibrated by melting high-purity indium, lead, and antimony. X-ray powder diffraction (XRPD) data were collected on a Rigaku RINT-2200 (Ultima) diffractometer using Cu Kα radiation. Scanning electron microscopy (SEM) was performed using a Hitachi S2500CX.

Kinetic Experiments. The desorption kinetic measurements were carried out using Rigaku Instrument TG8120 in a nitrogen flow (50 mL/min). The instrument kept the microvalance chamber in the isothermal condition, with sample (**3** ⊃ **2H$_2$O·2MeOH**): 12.717 mg (308 K), 11.833 mg (313 K), 13.105 mg (318 K), and 9.560 mg (323 K). The weight loss in the isothermal condition was monitored until the guest molecules were completely released. The fraction reacted in time (α) were calculated on the bases of the weight loss in time.

Single-Crystal X-ray Analysis. Single crystals of **1**, **2** ⊃ **2Me$_2$CO**, and **3** ⊃ **2H$_2$O·2MeOH** were mounted on a glass fiber and coated with epoxy resin. For each compound, X-ray data collection was carried out using a Rigaku Mercury diffractometer with graphite-monochromated Mo Kα radiation ($\lambda = 0.71069$ Å) and a CCD two-dimensional detector. The sizes of the unit cells were determined from reflections collected on the setting angles of six frames by changing ω by 0.5° for each frame. Two different χ settings were used. Intensity data were collected with a ω scan width of 0.5°. Empirical absorption correction using REQABA[11] was performed for all data. Crystal data and details of the structure determinations are summarized in Table 1. For **1**, the structure was solved by a direct method using the SIR97 program[12] and expanded using Fourier synthesis.[13] For **2** ⊃ **2Me$_2$CO**, the structure was solved by a Patterson method using the SAPI91 program[14] and expanded using Fourier synthesis.[13] For **3** ⊃ **2H$_2$O·2MeOH**, the structure was solved by a direct method using the SIR92 program[15] and expanded using Fourier synthesis.[13] The final cycles of the full-matrix least-squares refinements were based on all the observed reflections. All calculations were performed using the teXsan crystallographic software package of Molecular Structure Corp.[16] For all compounds, the non-hydrogen atoms were refined anisotropically and all the hydrogen atoms were placed in ideal positions. In compound **2** ⊃ **2Me$_2$CO**, the disorder of the acetone molecule containing O(2) and C(14)−C(16) was found at the final stage, and thus, its atom positions were isotropically refined under rigid conditions.

(11) Jacobson, R. A. *REQABA Empirical Absorption Correction*, Version 1.1-03019.98; Molecular Structure Corp.: The Woodlands, TX, 1996−1998.
(12) Altomare, A.; Burla, M. C.; Camalli, M.; Cascarano, G. L.; Giacovazzo, C.; Guagliardi, A.; Moliterni, A. G. G.; Polidori, G.; Spagna, R. *J. Appl. Crystallogr.* **1999**, *32*, 115−119.
(13) Beurskens, P. T.; Admiraal, G.; Beurskens, G.; Bosman, W. P.; deGelder, R.; Israel, R.; Smits, J. M. M. *The DIRDIF-94 program system*; Technical Report of the Crystallography Laboratory; University of Nijmegen: The Netherlands, 1994.
(14) Hai-Fu, F. *Structure Analysis Programs with Intelligent Control*; Rigaku Corp: Tokyo, 1991.
(15) Altomare, A.; Burla, M. C.; Camalli, M.; Cascarano, M.; Giacovazzo, C.; Guagliardi, A.; Polidori, G. *J. Appl. Crystallogr.* **1994**, *27*, 435.
(16) *teXsan Crystal Structure Analysis Package*; Molecular Structure Corp.: The Woodlands, TX, 2000.

Scheme 1

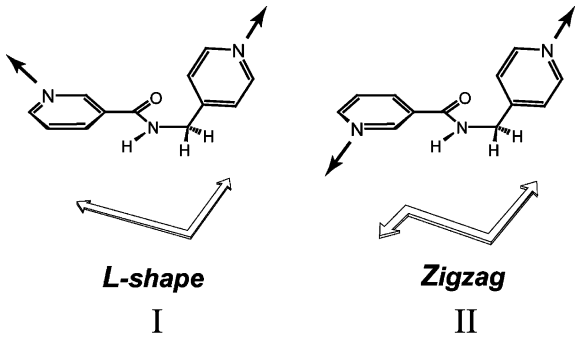

Results and Discussion

Design Principles. The 4-pmna ligand consists of two structural parts: (1) pyridyl groups, which can coordinate to a metal, and (2) an amide group, which can form hydrogen-bonding interactions with nitrogen and carbonyl oxygen atoms. Two pyridine groups (the carbonyl pyridine group (N^C) and the methylene pyridine group (N^M)) were utilized, connected by the amide and methylene moieties. Because of the π-conjugation between the carbonyl pyridine group and the amide moiety of the 4-pmna ligand, two types of coordinated direction were expected, depending on the N^C plane rotation (Scheme 1): type I, which is an L-shaped ligand, and type II, a zigzag-shaped ligand. Type II 4-pmna ligands act as straight bridging ligands, such as in 4,4′-bipyridine. On the other hand, for the L-shaped ligands such as in 2,4′-bipyridine[17] and 3,4′-bipyridine,[18] several network motifs (one-dimensional, two-dimensional, or three-dimensional) can be expected with a combination of metals and anions.

Crystal Structure of $[CoCl_2(4\text{-pmna})_2]_n$ (1). Figure 1a shows the coordination environment of the cobalt ion in **1**. The cobalt(II) center is octahedrally coordinated to the four nitrogen atoms of 4-pmna ligands in the equatorial plane, in which two types of nitrogen donors, N^C and N^M, are coordinated to the cobalt ion in a *trans* fashion. All of the Co−N bond distances are similar to each other: Co−N(1) = 2.208(2) Å and Co−N(2) = 2.237(2) Å. In addition, two Cl^- ions are coordinated axially with a bond distance of Co−Cl(1) = 2.447(1) Å. In **1**, the 4-pmna ligands are L-shaped. The cobalt ions are linked by 4-pmna ligands to form a one-dimensional chain with a repeated rhomboid motif. The amide planes are perpendicular to the planes of the rhomboid-shaped cavities, and each repeated rhomboid-type chain is connected along the ($b + c$) direction by hydrogen bonds between the amide moiety and the Cl^- ion (N−Cl = 3.274(3) Å) (Figure 1b). The nearest Co−Co distance is about 12.0 Å in the chain and 7.9 Å between the adjacent chains.

$\{[Co(NCS)_2(4\text{-pmna})_2]\cdot 2Me_2CO\}_n$ (2 ⊃ $2Me_2CO$). Figure 2a shows the coordination environment of the cobalt ion in **2** ⊃ **$2Me_2CO$**. The cobalt(II) center is octahedrally coordinated to the six nitrogen atoms of the 4-pmna ligands and the two NCS groups. In the equatorial plane, the N^C and N^M atoms of the 4-pmna ligands are coordinated to the cobalt ion in a *trans* fashion. All of the Co−N bond distances are similar to each other: Co−N(1) = 2.218(3) Å and Co−N(2) = 2.203(3) Å. In addition, the NCS groups are coordinated axially in a bent

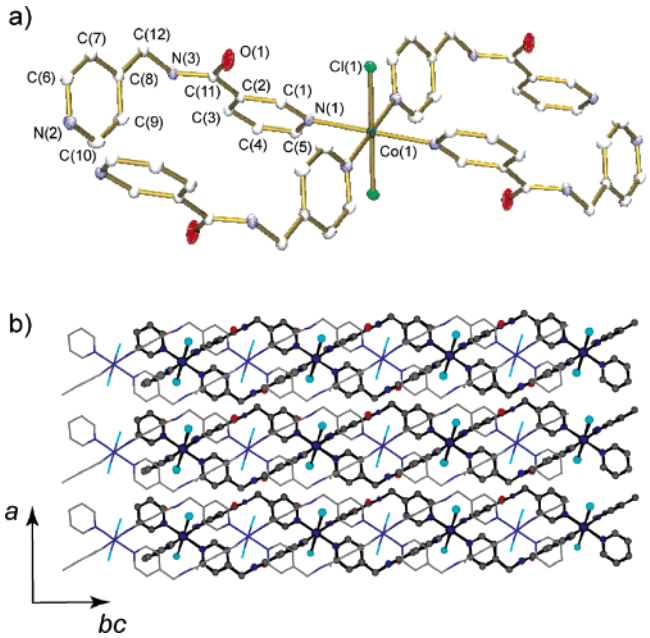

Figure 1. Crystal structure of $[CoCl_2(4\text{-pmna})_2]_n$ (**1**). (a) ORTEP drawing of **1** at the 30% probability level. Hydrogen atoms are omitted for clarity. (b) Overall structure of **1**. Repeated rhomboid-type chains connected by Cl−HN hydrogen bonds. Two chains stack in a staggered manner, and the thin and thick lines show the upper and lower chains, respectively.

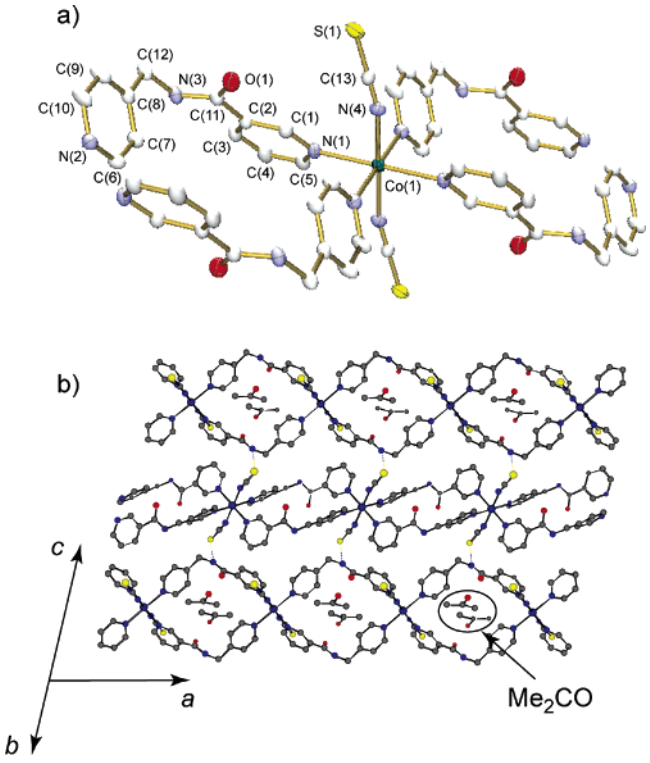

Figure 2. Crystal structure of $\{[Co(NCS)_2(4\text{-pmna})_2]\cdot 2Me_2CO\}_n$ (**2** ⊃ **$2Me_2CO$**). (a) ORTEP drawing of **2** ⊃ **$2Me_2CO$** at the 30% probability level. Hydrogen atoms and acetone molecules are omitted for clarity. (b) Overall structure of **2** ⊃ **$2Me_2CO$**. Three repeated rhomboid-type chains are connected by S−HN hydrogen bonds and included acetone molecules.

(17) (a) Liu, C. M.; Zhang, D. Q.; Zhu, D. B.; Jin, X. *Trans. Met. Chem.* **2003**, *28*, 336−338. (b) Tong, M. L.; Chen, X. M.; Ye, B. H.; Ng, S. W. *Inorg. Chem.* **1998**, *37*, 5278−5281.

(18) (a) Fun, H. K.; Raj, S. S. S.; Xiong, R. G.; Zuo, J. L.; Yu, Z.; Zhu, X. L.; You, X. Z. *J. Chem. Soc., Dalton Trans.* **1999**, 1711−1712. (b) LaDuca, R. L., Jr.; Desiak, M.; RarigJr, R. S.; Zubieta, J. *Inorg. Chim. Acta* **2002**, *332*, 79−86.

fashion at an angle of 165.0(2)° (Co(1)−N(4)-C(13)). The *trans* N−Co−N bond angles for the NCS and pyridine ligands are 180°. The *cis* N−Co−N bond angles are in the range 87−93°, implying a distorted octahedral environment. The cobalt ions are linked by L-shaped 4-pmna ligands to form a one-dimensional chain with a repeated rhomboid motif in a similar manner to compound **1**. Each repeated rhomboid chain is connected by a hydrogen bond between the amide moiety and the sulfur atom of the NCS group (N−S = 3.361(2) Å) (Figure 2b). In the repeated rhomboid chain, two L-shaped 4-pmna ligands form cavities with a cross-sectional area of 3.3 × 2.7 Å^2,[19] which is occupied by acetone molecules. Within each chain, the acetone molecules are accommodated without any significant interaction occurring with any atom. The volume fraction occupied by the solvent molecules was estimated to be 30% of the total crystal volume.[20] The nearest Co−Co bond distance is about 11.4 Å in the chain and 9.8 Å between adjacent chains.

{[Co(4-pmna)$_2$(H$_2$O)$_2$](NO$_3$)$_2$·2CH$_3$OH}$_n$ (3 ⊃ 2H$_2$O·2MeOH). Figure 3a shows a coordination environment of the cobalt ion in **3 ⊃ 2H$_2$O·2MeOH**. The cobalt(II) center is octahedrally coordinated to the four nitrogen atoms of the 4-pmna ligands in the equatorial plane, in which the N^C and N^M are coordinated to the cobalt ion in a *trans* fashion. All of the Co−N bond distances are similar to each other: Co−N(1) = 2.187(2) Å and Co−N(2) = 2.203(2) Å. In addition, the H$_2$O molecules are coordinated axially with a bond distance of 2.082-(2) Å. The cobalt ions are linked by the 4-pmna ligands to form a one-dimensional chain with a repeated rhomboid motif, similar to that observed in compounds **1** and **2 ⊃ 2Me$_2$CO**. Each chain is connected by hydrogen bonds *via* nitrate anions, as shown in Figure 3c. In the repeated rhomboid chain, the two L-shaped 4-pmna ligands form a cavity with a cross-sectional area of 3.6 × 3.0 Å^2, which is occupied by methanol molecules. The methanol molecules are hydrogen bonded to the oxygen atoms of the amide moieties (O(MeOH)−O(1) = 2.724(3) Å) and to coordinated H$_2$O molecules (O(MeOH)−O(2) = 2.694(3) Å). The volume fraction occupied by the solvent molecules was estimated to be 16% of the total crystal volume.[20] The nearest Co−Co distance was about 11.4 Å in the chain and 8.1 Å between adjacent chains.

The crystal structures of all three compounds comprise a "repeated rhomboid-type chain" motif.[4k,21,22] Their similar crystal structures originate in the similar torsion angles between the carbonyl pyridine, the methylene pyridine, and the amide plane in compounds **1**−**3**.

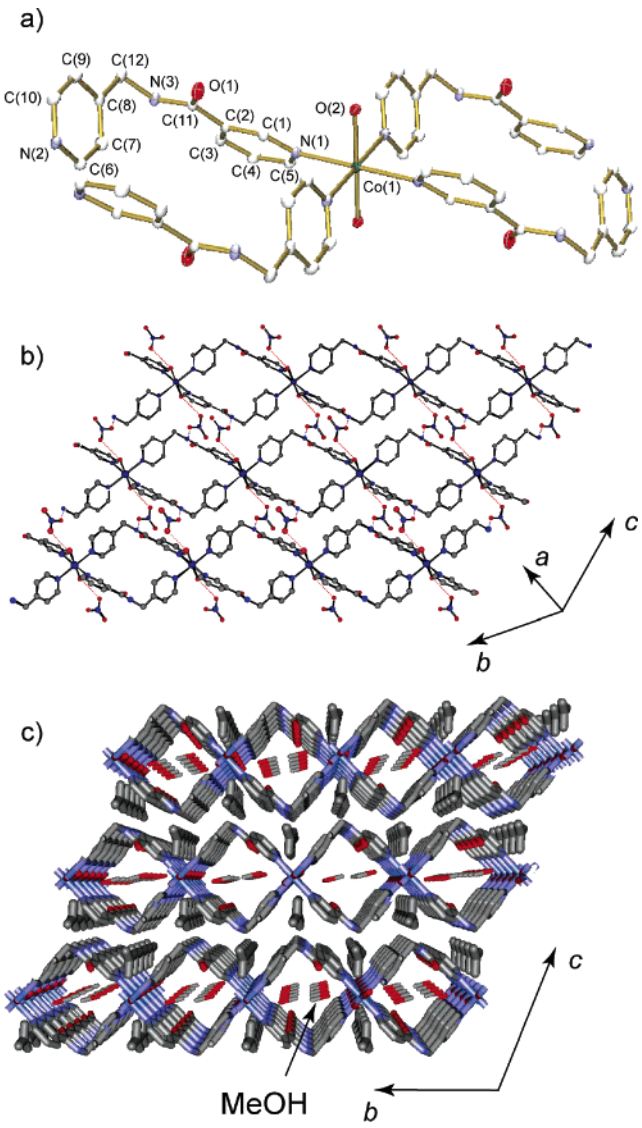

Figure 3. Crystal structure of {[Co(4-pmna)$_2$(H$_2$O)$_2$](NO$_3$)$_2$·2CH$_3$OH}$_n$ (**3 ⊃ 2H$_2$O·2MeOH**). (a) ORTEP drawing of **3 ⊃ 2H$_2$O·2MeOH** at the 30% probability level. Hydrogen atoms, nitrate anions, and methanol molecules are omitted for clarity. (b) Overall structure of **3 ⊃ 2H$_2$O·2MeOH**. A repeated rhomboid-type chain of **3 ⊃ 2H$_2$O·2MeOH** including methanol molecules with hydrogen bonds. (c) Overall structure of **3 ⊃ 2H$_2$O·2MeOH** along the *a*-axis. Three repeated rhomboid-type chains are connected by O(H$_2$O)−NO$_3$−N(amide) hydrogen bonds.

In all three compounds, the Co(II) metal centers adopt an octahedral geometry and coordinate with the 4-pmna ligands in a ratio of 1:2 to afford the rhomboid-shaped cavities surrounded by pyridine panels having dimensions of about 8.0 × 6.5 Å^2. Despite the similarity of the motif comprising the network, the mutual relationships between the chains are different in compounds **1**−**3** (Scheme 2). The face-to-face stacking produces a channel for guest molecule incorporation, as observed in **3 ⊃ 2H$_2$O·2MeOH**.

The introduction of hydrogen bonds into the coordination polymers provides a framework flexibility,[3b] and a py-amide-py type ligand is suitable for the rational introduction of hydrogen bonds. Since metal ions prefer the pyridyl group (py) relative to the amide group, the py groups at both ends are used for the formation of the framework backbone, and the amide groups serve as the connectors between each network motif.[5]

(19) The size is measured by considering van der Waals radii for constituting atoms. Hereafter, all the size estimations of pore are made in this way.
(20) Speck, A. L. PLATON, A. M. C. T. Utrecht University, Utrecht, The Netherlands, 1999.
(21) (a) Fujita, M.; Kwon, Y. J.; Miyazawa, M.; Ogura, K. *J. Chem. Soc., Chem. Commun.* **1994**, 1977−1978. (b) Kasai, K.; Aoyagi, M.; Fujita, M. *J. Am. Chem. Soc.* **2000**, *122*, 2140−2141. (c) Sharma, C. V. K.; Diaz, R. J.; Hessheimer, A. J.; Clearfield, A. *Cryst. Eng.* **2000**, *3*, 201−208. (d) Kondo, M.; Shimamura, M.; Noro, S. i.; Kimura, Y.; Uemura, K.; Kitagawa, S. *J. Solid State Chem.* **2000**, *152*, 113−119. (e) Zaman, M. B.; Udachin, K.; Ripmeester, J. A.; Smith, M. D.; Loye, H.-C. z. *Inorg. Chem.* **2005**, *44*, 5047−5059.
(22) According to our previous category about "metallo-amino acid" regarded NH-py-M-py-CO unit as "amino acid fragment", compounds **1**−**3** are symbolized as C[Co^{II}(p^1, m^0)] (see ref 3b). In the case of Co^{II} and other py-CONH-X-py ligands, *N*-3-pyridylisonicotinamide (3-pia), *N*-3-pyridylnicotinamide (3-pna), and *N*-(2-pyridin-4-ylethyl)isonicotinamide (4-peia), the symbols are L[Co^{II}(m^0, p^0)], L[Co^{II}(m^0, m^0)], and L[Co^{II}(p^2, p^0)], respectively (ref 5). Interestingly, the control of (n^i, c^j) induce the different overall structure (in this case C (chain)).

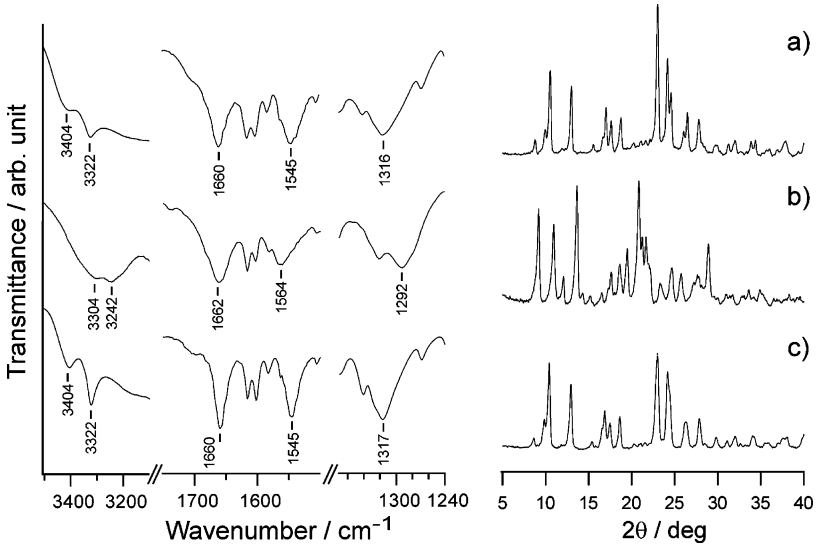

Figure 4. IR spectra (left) and XRPD patterns (right) of (a) as-synthesized **3** ⊃ **2H$_2$O·2MeOH**, (b) **3** obtained by drying in vacuo for 20 h at 373 K, and (c) **3** ⊃ **2H$_2$O·2MeOH** obtained by exposing **3** to methanol/H$_2$O vapor (v/v 1:1) for 4 days.

Scheme 2

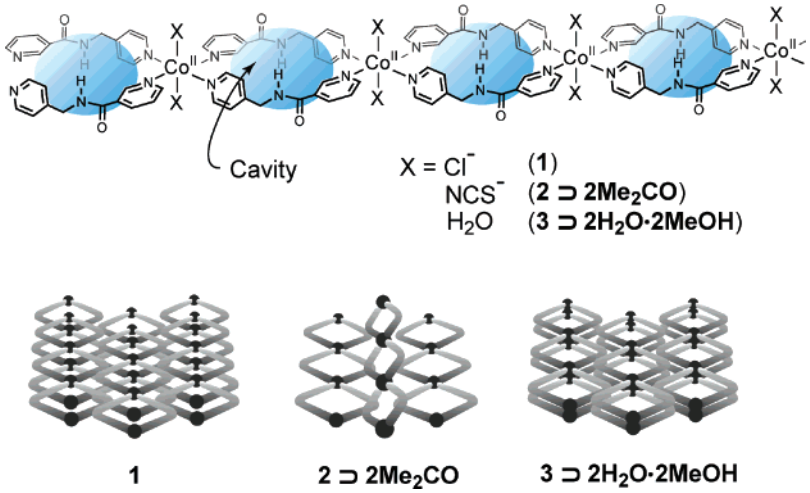

Two types of hydrogen bonds were observed in the coordination polymers: one was used to bond to the guest molecule, and the other was hydrogen bonding within the framework backbone. Hereafter, based on this new system, we will demonstrate a reversible structural change corresponding to the guest molecule adsorption and desorption.

Reversible Structural Changes Induced by Guest Molecule Desorption and Adsorption. The removal of guest molecules causes a significant change in the framework of **3** ⊃ **2H$_2$O·2MeOH**. Compound **3** was obtained by treating **3** ⊃ **2H$_2$O·2MeOH** under reduced pressure at 100 °C.[23] The formation of **3** was readily detected using X-ray powder diffraction (XRPD) and IR spectroscopy. The sharp diffraction pattern of **3** demonstrates the formation of a new crystalline form, whose structure was different from that of **3** ⊃ **2H$_2$O·2MeOH** (Figure 4b, right panel). Upon exposure to methanol/H$_2$O vapor (v/v 1:1), the original crystal structure was recovered, as confirmed by the coincidence of the peak positions and relative intensities. Note that the diffraction pattern shown in Figure 4c is in good agreement with that calculated from the single-crystal data of **3** ⊃ **2H$_2$O·2MeOH**.[24]

IR spectroscopy also provides information on the crystal structure of **3**. The O−H stretching band of the solvent, the N−H stretching band of the amide moieties, and the amide-I and amide-II bands appear in the 3650−3200, 3500−3100, and 1700−1500 cm^{-1} regions, respectively.[25] The amide moieties in **3** ⊃ **2H$_2$O·2MeOH** provide structured bands, as shown in Figure 4a: O−H stretching, N−H stretching, and amide-I and

(23) Two methanol and two coordinated H$_2$O molecules are desorbed, which is monitored by the elementary analysis and TG, as discussed in the next paragraph.

(24) As shown in Figures S2 and S3 (Supporting Information), XRPD and TG measurements for **2** ⊃ **2Me$_2$CO** were also carried out. At room temperature, as prepared **2** ⊃ **2Me$_2$CO** immediately decomposed to be amorphous form. Two major reasons for such instability could be considered: (i) the mutual relationship among the chains in **2** ⊃ **2Me$_2$CO** is not face-to-face stacking without straight one-dimensional channel, and (ii) guest molecules (Me$_2$-CO) without significant interactions to the framework are easy to release from the cavities. Unfortunately, such a compound is not suitable for our mentioned thermal approach (in the next paragraph in the text) due to the difficulties in strict measurements.

(25) (a) Nakamoto, K. *Infrared and Raman Spectra of Inorganic and Coordination Compounds*, 5th ed.; Wiley: New York, 1997. (b) Bellamy, L. J. *Advances in Infrared Group Frequencies*; Methuen: London, 1968. (c) Ghadiri, M. R.; Granja, J. R.; Milligan, R. A.; McRee, D. E.; Khazanovich, N. *Nature* **1993**, *366*, 324−327. (d) Haris, P. I.; Chapman, D. *Biopolymers* **1995**, *37*, 251−263. (e) Hartgerink, J. D.; Granja, J. R.; Milligan, R. A.; Ghadiri, M. R. *J. Am. Chem. Soc.* **1996**, *118*, 43−50.

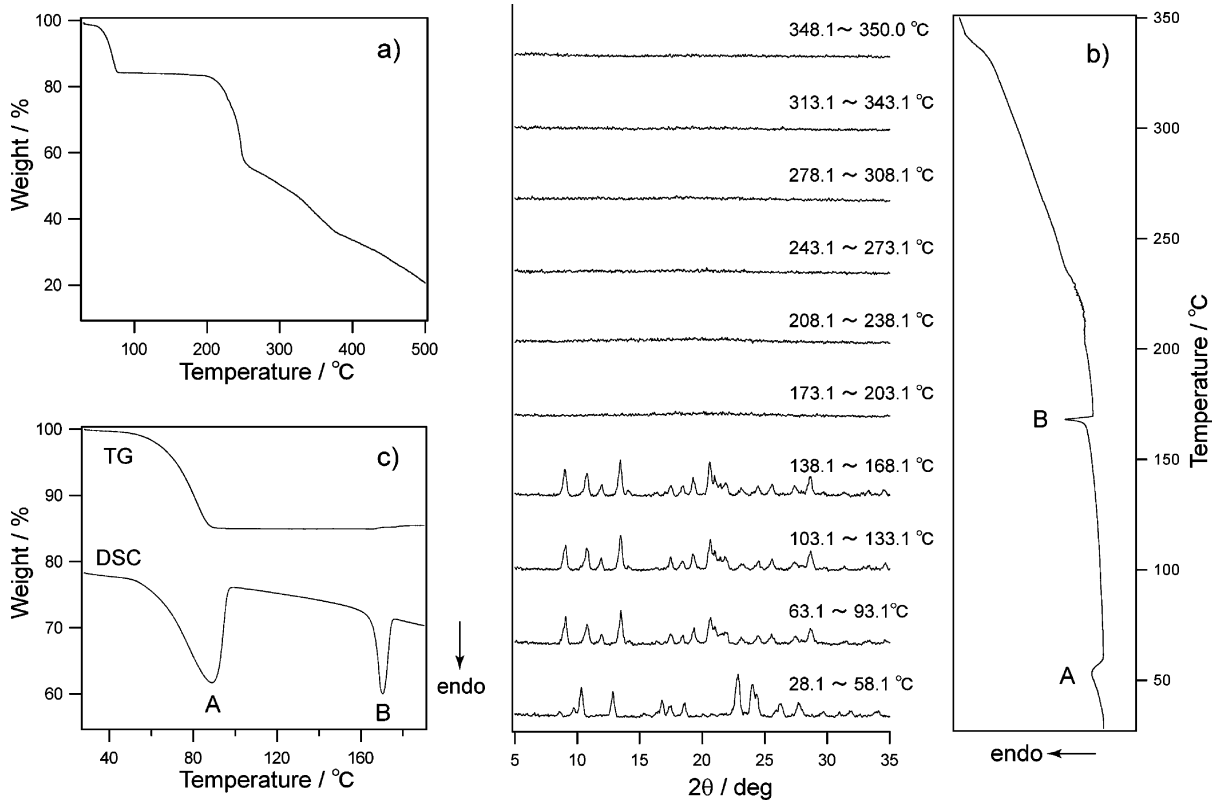

Figure 5. (a) TG analysis of **3** ⊃ **2H₂O·2MeOH** over the temperature range from 25 to 500 °C in a nitrogen flow (50 mL/min), (b) simultaneously XRPD and DSC measurements of **3** ⊃ **2H₂O·2MeOH** over the temperature range from 28.1 to 350.0 °C at a heating rate of $\beta = 1$ °C/min in a nitrogen flow (50 mL/min), and (c) TG and DSC thermograms of **3** ⊃ **2H₂O·2MeOH** over the temperature range from 30 to 190 °C at a heating rate of $\beta = 5$ °C/min in a nitrogen flow (50 mL/min).

Scheme 3

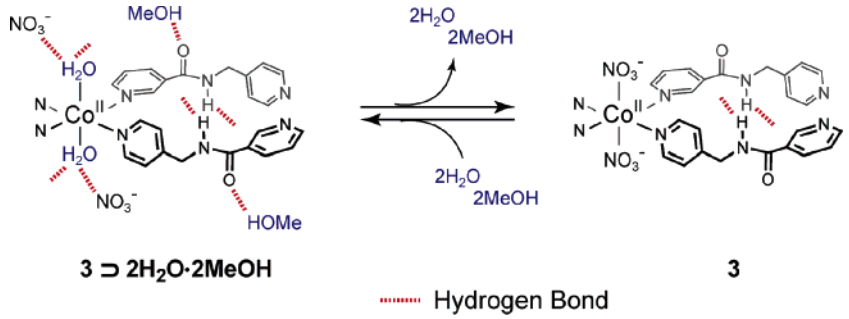

amide-II bands were observed at 3404, 3322, 1660, and 1545 cm^{-1}, respectively. The following bands were observed in **3**: N−H stretching vibrations at 3304 and 3242 cm^{-1}, the amide-I band at 1662 cm^{-1}, and the amide-II band at 1564 cm^{-1}. The IR data indicate the formation of strong hydrogen bonds by the 4-pmna ligands, since the stretching and bending modes were shifted to lower and higher frequencies, respectively.

The IR data from the N−O stretching band of the NO_3^- ions also provide information on the environment of these ions in **3**.[25a] In the desorption process, the N−O stretching band changed from 1316 (**3** ⊃ **2H₂O·2MeOH**) to 1292 cm^{-1} (**3**), indicating that the NO_3^- anions were coordinated to the cobalt(II) atoms instead of the H_2O molecules (Scheme 3). The N−O stretching band also demonstrates structural regeneration, because all the main bands in the regenerated structure were similar to those of the original **3** ⊃ **2H₂O·2MeOH**.

Thermal Gravimetry, Differential Thermal Analysis, and Energetics. Figure 5a shows the thermogram of **3** ⊃ **2H₂O·2MeOH** in the temperature range 30−500 °C for a heating rate $\beta = 5$ °C/min. In the temperature range of 50−90 °C, the thermogram of **3** ⊃ **2H₂O·2MeOH** showed a mass loss corresponding to two methanol and two coordinated H_2O molecules (observed = 15.0%, calculated = 14.1%). The resulting adduct, **3**, was stable up to 170 °C, where it apparently melted (Endothermal peak B) and then gradually decomposed to form an amorphous phase with the loss of the 4-pmna ligands, as shown in the XRPD data with $\beta = 1$ °C/min (Figure 5b).

The DSC curve of **3** ⊃ **2H₂O·2MeOH** also indicates that the guest molecule was lost in a single endothermic step (Figure 5c, peak A), with an enthalpy change $\Delta H_A = -198$ kJ/mol. This was followed by the emergence of peak B, an endotherm with $\Delta H_B = -40$ kJ/mol, without any associated weight loss. Considering the data collected from the XRPD, IR, TG, and

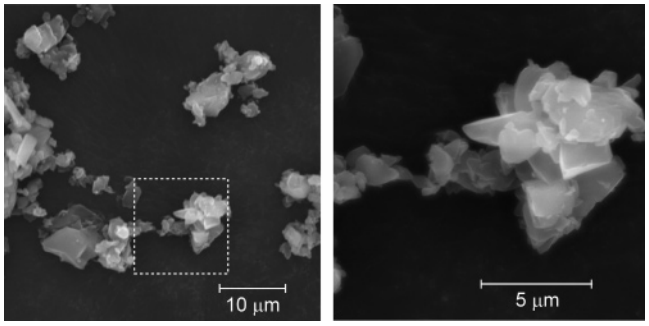

Figure 6. SEM images of as-synthesized **3** ⊃ **2H$_2$O·2MeOH**. The left image is expanded corresponding to the dashed square in the right image.

DSC experiments, the adsorption and desorption processes of **3** ⊃ **2H$_2$O·2MeOH** are as shown in eq 2

$$\mathbf{3} \supset \mathbf{2H_2O{\cdot}2MeOH}(s) \rightleftarrows \mathbf{3}(s) + 2H_2O(g) + 2MeOH(g), \Delta H_A \quad (2)$$

where the reaction shown in eq 2 involves an enthalpy change, ΔH_A. The main contributions to ΔH_A are from the vaporization enthalpies of H_2O (43.99 kJ/mol) and methanol (37.43 kJ/mol).[26] It was considered that the excess enthalpy (≈35 kJ/mol) corresponded to ΔH_{clath}. This magnitude is similar to that previously estimated in other systems, e.g., 31 and 25 kJ/mol for $\{[Co(NCS)_2(3\text{-pia})_2]\cdot 4Me_2CO\}_n$[5c] and $\{[Co(NCS)_2(4\text{-peia})_2]\cdot 4Me_2CO\}_n$,[5b] respectively.[27]

Desorption Kinetics and Deduction of the Particle Size. The reaction kinetics in the solid state are influenced by the basic reaction mechanism and also by other factors, such as the particle size distribution.[28] Figure 6 shows SEM images of microcrystals of **3** ⊃ **2H$_2$O·2MeOH**. Since these microcrystals were stacked in a random fashion, it was impossible to estimate the crystal size distribution using SEM. However, it was possible to deduce the particle size distribution from the kinetic data. The kinetic data at different temperatures are shown in Figure 7a, where α denotes the fraction reacted at a time *t*.

The adsorption and desorption of a guest molecules proceeds along a given direction because of the structural one-dimensionality of the nanopores in **3** ⊃ **2H$_2$O·2MeOH**. The adsorption and desorption reactions originate from the surface and proceed along the channel, irrespective of any diffusion-limited mechanism or the interface-limited mechanism. If the shape of the crystal is infinitely long along the channel, then the kinetic constant remains constant during the absorption and desorption reactions; however, the real system consists of many particles with different channel lengths. Each particle contributes to the reacted fraction from the common contribution per unit sectional area of the channel only, before the reaction covers the particle. Thus, the appropriate defined reaction rate is directly proportional to the total sectional area (normal to the channel) available at time *t*.

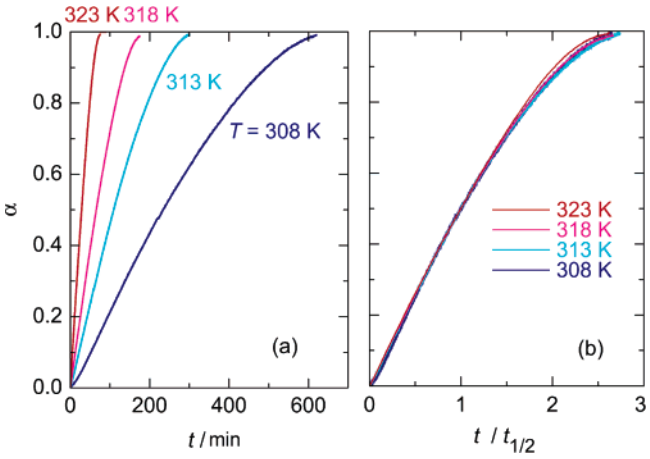

Figure 7. (a) Plots of α vs *t* for the process of "**3** ⊃ **2H$_2$O·2MeOH** → **3**" at 308, 313, 318, and 323 K in a nitrogen flow (50 mL/min). (b) Plots against the reduced rime.

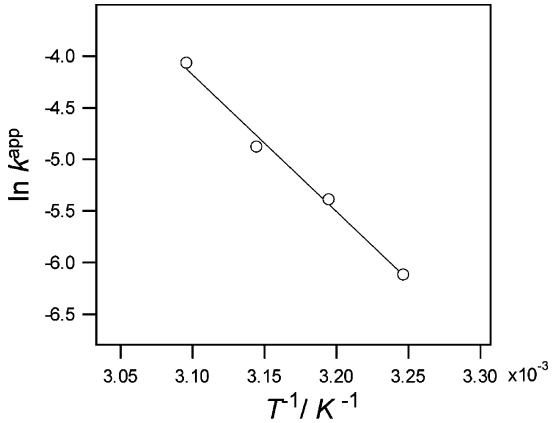

Figure 8. Arrenius plot (ln k^{app} vs T^{-1}) for desorption process of **3** ⊃ **2H$_2$O·2MeOH** in the isothermal condition (308, 313, 318, and 323 K), where k^{app} values are 2.20, 4.54, 7.58, and 17.1 (10^{-3} min^{-1}) at 308, 313, 318, and 323 K, respectively.

The above analysis assumes that the reaction process is described by a single reaction mechanism. This assumption can be verified by comparing the kinetic data at different temperatures. If two mechanisms act simultaneously, then the reaction will show a different temperature dependence because of the different activation energies for each mechanism. In contrast, if the assumption is valid, then the data can be reduced to a single curve by normalizing at a given time (such as $t/t_{1/2}$, where $t_{1/2}$ is the time when the reacted fraction is $t = 1/2$). Such a plot is shown in Figure 7b. The observed coincidence is acceptable and indicates that a single mechanism occurs during the desorption of **3** ⊃ **2H$_2$O·2MeOH** → **3**.

Since the uniqueness of the reaction mechanism has been established, the activation energy for the reaction **3** ⊃ **2H$_2$O·2MeOH** → **3** can be obtained by plotting the logarithm of the time at the same reacted fraction versus the reciprocal of the temperature without any assumption concerning the reaction mechanism. The plot shown in Figure 8 indicates that the activation energy was ca. 100 kJ mol^{-1}.[29]

The next step in deducing the channel length distribution was to determine the basic mechanism of the reaction. If a single crystal were used in our experiments, the reacted fraction would

(26) Weast, R. C.; Astle, M. J.; Beyer, W. H. *CRC Handbook of Chemistry and Physics*, 80th ed; CRC Press: Boca Raton, 1999.
(27) Earlier studies reported that the closed-to-open phase transformation enthalpies of the host (ΔH_{trans}) are 1.31(5) and 3.5(1) kJ/mol in β-[CuL_2] (L = $\{CF_3COCHCOC(CH_3)_2OCH_3\}^-$)[2b] and [$Ni(4\text{-MePy})_4(NCS)_2$],[2a] respectively. The equation[2a] $\Delta H_{clath} = \Delta H_{trans} + \Delta H_{sorp}$, where ΔH_{sorp} is the heat of adsorption, makes it possible to estimate ΔH_{trans} in this system. However, it is difficult to estimate ΔH_{sorp} in our system.
(28) (a) Gotor, F. J.; Criado, J. M.; Malek, J.; Koga, N. *J. Phys. Chem. A* **2000**, *104*, 10777−10782. (b) Sorai, M.; Atake, T.; Inaba, A.; Saito, K.; Hashimoto, T.; Kidokoro, S.; Oguni, M.; Ozao, R.; Tsuji, T.; Yokokawa, H.; Yoshida, H. *Comprehensive Handbook of Calorimetry and Thermal Analysis*; John Wiley & Sons Ltd.: Chichester, UK, 2004.

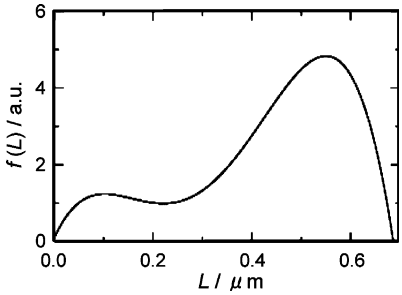

Figure 9. Distribution function of channel-length deduced from the isothermal kinetic data for desorption **3** ⊃ **2H$_2$O·2MeOH** → **3** in Figure 7.

increase in proportion to the reaction time (i.e., the reacted fraction ∝ $k_i t$) in the case of interface-limited reactions, whereas it would be proportional to the square- root of the time (i.e., the reacted fraction ∝ $k_d t^{1/2}$) in diffusion-limited cases. Since there was a characteristic particle size in our samples, some part of the kinetic data was expected to show either of the two mechanisms. Indeed, the kinetic data plot of **3** ⊃ **2H$_2$O·2MeOH** → **3** shown in Figure 7 is almost linear with respect to time between the reaction rate of 0.2 and 0.5. This strongly implies that desorption proceeded as a surface-limited zero-order reaction.[30] Considering the appearance of the second crystalline form upon desorption, it seems reasonable to deduce that a surface-limited mechanism occurred. The desorbed molecules immediately escaped into the gas phase, and there was no need to supply any molecules. This resulted in a zero-order reaction.

The apparent kinetic constant (k_i^{app} or k_d^{app}) was obtained as a function of time from the experimental data. This constant is related to the kinetic constant for an infinitely long complex (k) from

$$k^{app}(t) = k \int_{L(t)}^{\infty} f(l)\mathrm{d}l = k \int_{t}^{\infty} f[l(t)] \frac{\mathrm{d}l}{\mathrm{d}t} \mathrm{d}t \qquad (3)$$

where $f(l)$ is the channel-length distribution function. It is noted that no information was available concerning the real length scale from the kinetic data. The XRPD observation indicated that a typical length of the particles of **3** ⊃ **2H$_2$O·2MeOH** was 0.55 μm.[31] By fixing the length scale to this length as being that of the most frequent channel length, the channel-length distribution function can be obtained, as shown in Figure 9.

As the channel length distribution function is deduced by differentiating twice with respect to time, $\alpha(t)$, the major peak in the distribution was unsymmetrical, i.e., there was a steeper decrease on the longer side.

The analysis given here was based on the structural anisotropy of the nanopores, and this method is superior to the standard methods used in the analysis of solid-state reactions in some respects. The first point concerns the use of isothermal data. It is widely accepted that isothermal data are more reliable than dynamical data in thermal analysis, although more time-consuming. The second point is that this method offers a way to confirm the uniqueness of the reaction mechanism. Although this uniqueness is assumed implicitly in any analytical method utilizing thermal analysis, no method offers a way to confirm the validity of this assumption. The third point is that this method is the first to provide information on the channel length distribution. The basic idea of deducing the channel length distribution should be applicable irrespective of the basic mechanism of reaction. An extension of the analytical method is now underway by one of the authors.

(29) It was also possible to obtain the activation energy (E_{de}) by the Ozawa−Flynn−Wall and Kissingers method on the basis of TG and DTA measurements with different heating rates: (a) Flynn, J. H.; Wall, L. A. *J. Polym. Sci. B* **1966**, *4*, 323−328. (b) Ozawa, T. *Bull. Chem. Soc. Jpn.* **1965**, *38*, 1881−1886.

(30) Several models were adapted, as shown in Figure S5 (Supporting Information).

(31) The particle size of as-prepared **3** ⊃ **2H$_2$O·2MeOH** is estimated by the Scherrer equation using XRPD measurements: Klug, H. P.; Alexander, L. E. *X-ray diffraction procedures for polycrystalline and amorphous materials*; Wiley: New York, 1954.

Conclusion

This work was devoted to two major subjects: (i) the synthesis and analysis of coordination polymers with 4-pmna ligands that included hydrogen-bonding sites orientated toward the porous frameworks and (ii) the characterization of the adsorption/desorption process on **3** ⊃ **2H$_2$O·2MeOH** with subsequent kinetic and thermodynamic analysis.

(i) Using cobalt(II) and 4-pmna ligands, we succeeded in producing three novel coordination polymers **1**−**3**. In all three compounds, the cobalt(II) atoms are bridged by L-shaped 4-pmna ligands forming repeated rhomboid networks. The mutual relationships between the repeated rhomboid chains are regulated by the hydrogen bonds occurring between the anions and the amide moieties in the 4-pmna ligands, to attain one-dimensional micropores in **3** ⊃ **2H$_2$O·2MeOH**. Guest molecules are bound with hydrogen bonds in these micropores, where the structural transformation (**3** ⊃ **2H$_2$O·2MeOH** ↔ **3**) was induced by the adsorption and desorption of a guest molecule.

(ii) Kinetic and thermodynamic analysis was carried out on **3** ⊃ **2H$_2$O·2MeOH**. The clathration enthalpy (≈35 kJ/mol) was successfully obtained from DSC data. The desorption of **3** ⊃ **2H$_2$O·2MeOH** under isothermal conditions proceeded via a single reaction mechanism involving a surface-limited zero-order reaction. In addition, we succeeded in estimating the unsymmetrical channel length distribution of **3** ⊃ **2H$_2$O·2MeOH** as being 0.55 μm.

This research is particularly relevant to the construction of porous coordination polymers utilizing both coordination and hydrogen bonds, since the rational design of solids has important ramifications for the development of new materials. Many porous coordination polymers have been synthesized and reported. However, to the best of our knowledge, reports on the kinetic and thermodynamic measurements on these materials are sparse. We anticipate that this study will be useful for analyzing the thermal behavior of porous coordination polymers.

Acknowledgment. This work was supported by a Grant-in-Aid for Scientific Research on Priority Area (No. 434, "Chemistry of Coordination Space") and Young Scientist (B) (No. 17750058) from the Ministry of Education, Science, Sports and Culture, Japan.

Supporting Information Available: XRPD simulation, estimation of the activation energy on "**3** ⊃ **2H$_2$O·2MeOH** → **3**" using the Ozawa−Flynn−Wall and Kissinger methods, several kinetics models applied to the desorption of **3** ⊃ **2H$_2$O·2MeOH**, and X-ray crystallographic files (CIF) for **1**−**3**. This material is available free of charge via the Internet at http://pubs.acs.org.

JA064152R